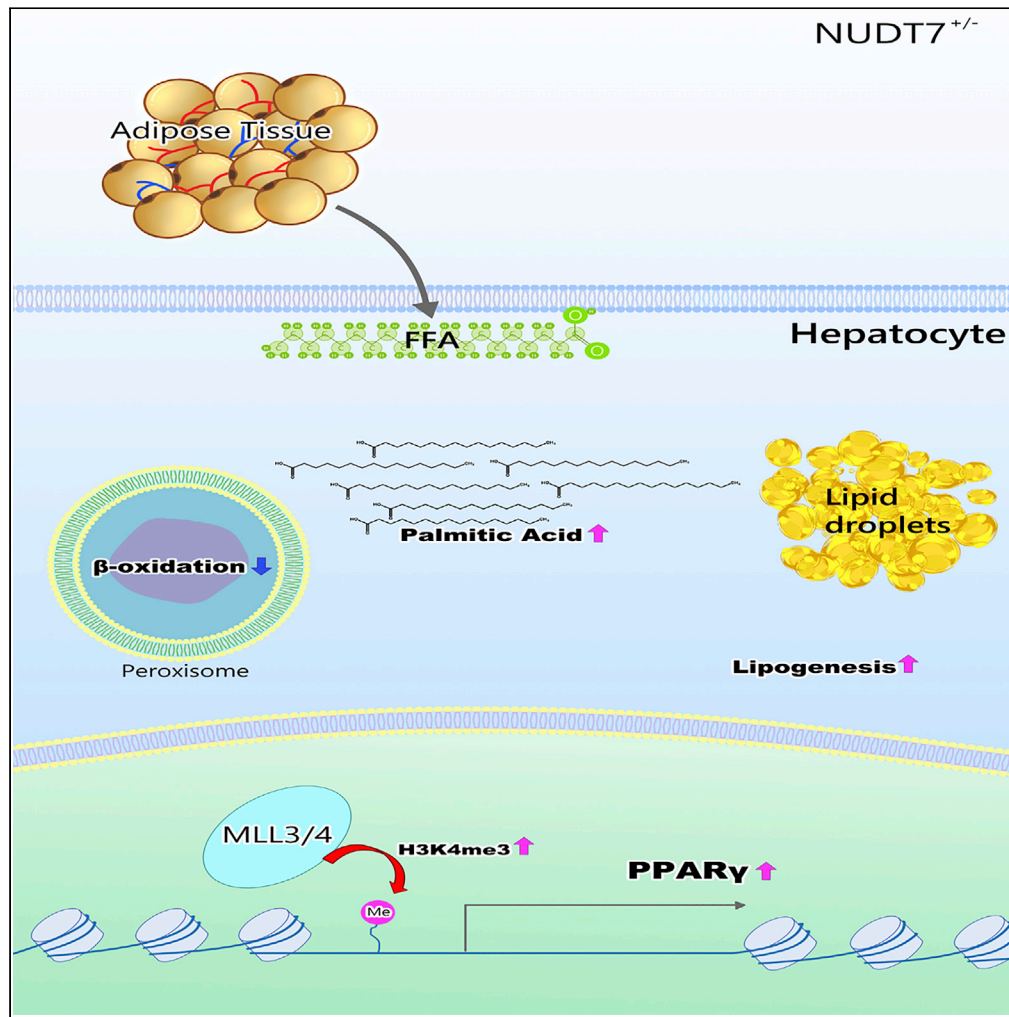## Article

Deficiency of peroxisomal NUDT7 stimulates *de novo* lipogenesis in hepatocytes

Jinsoo Song, In-Jeoung Baek, Sujeong Park, ..., Hye Won Lee, Byoung Kuk Jang, Eun-Jung Jin

jineunjung@wku.ac.kr

Highlights

Peroxisomal dysfunction is involved in the pathogenesis of NAFLD

Heterozygous peroxisomal Nudt7$^{+/-}$ mice develop NAFLD via activation of PPAR signaling

Palmitic acid accumulated by NUDT7 deficiency stimulates H3K4me3 on Pparg promoter

Liraglutide attenuates hepatic DNL induced by NUDT7 deficiency

Article

Deficiency of peroxisomal NUDT7 stimulates *de novo* lipogenesis in hepatocytes

Jinsoo Song,[1,2] In-Jeoung Baek,[3] Sujeong Park,[1] Jinjoo Oh,[1] Deokha Kim,[1] Kyung Song,[4] Mi Kyung Kim,[5] Hye Won Lee,[6] Byoung Kuk Jang,[5] and Eun-Jung Jin[1,2,7,*]

SUMMARY

Here, we found that heterozygous null of peroxisomal *Nudt7* (*Nudt7*^{+/−}) induced the typical NAFLD features, *i.e.* increased levels of hepatic triglyceride (TG) and fatty acid (FA), infiltration of inflammatory cells, impaired glucose tolerance and insulin sensitivity, and stimulation of lipolysis from adipose tissue. Particularly, in *Nudt7*^{+/−} hepatocytes, *de novo* lipogenesis (DNL) was significantly increased. Ingenuity pathway analysis (IPA) and KEGG pathway analysis of RNA sequencing data suggested the activation of PPAR signaling in the liver of *Nudt7*^{+/−} mice. Moreover, accumulation of palmitic acid in *Nudt7*^{+/−} hepatocyte increased the level of H3K4me3 on the promoters of PPARγ resulting in the activation of PPARγ and induced the DNL in the hepatocytes of *Nudt7*^{+/−} mice. Moreover, we found that liraglutide significantly reduced typical NAFLD features induced by NUDT7 deficiency. Our data suggest that dysregulation of peroxisomal NUDT7 is responsible for upregulation of hepatic DNL by accumulation of palmitic acid and PPARγ activation.

INTRODUCTION

The earliest stage of nonalcoholic fatty liver disease is liver steatosis, which is characterized by the fat accumulation, inflammation, and fibrosis in hepatocytes, and potentially progresses to cirrhosis and hepatocellular carcinoma (Farrell and Larter, 2006; Benedict and Zhang, 2017). Since fatty liver has become an epidemic problem worldwide recently, understanding the underlying molecular and signaling mechanisms of hepatic fat accumulation will be a stepping stone for developing the potential therapeutic approaches and strategy to control the pathogenesis of fatty liver.

Dysregulation of hepatic lipid metabolism due to imbalance in fatty acid synthesis, storage, and catabolism closely linked to the development of fatty liver (Musso et al., 2009; Gong et al., 2017). The level of hepatic lipid could be governed by the balance between lipid acquisition through the uptake of circulating fatty acids (FA), lipid disposal through lipid oxidation or export, and/or *de novo* lipogenesis (DNL) (Fabbrini et al., 2010) by the complicated interactions among hormones, nuclear receptors, and transcription factors. Uptaking circulating FA in hepatocyte is affected by fatty acid transport proteins (FATPs), fatty acid translocase (CD36/FAT) (Chao et al., 2000), and fatty acid binding protein (FABP)1 (Wang et al., 2015) and exporting hepatic lipids are induced by microsomal triglyceride transfer protein (MTTP) and apolipoprotein B (apoB) to reduce hepatic lipid content (Hui et al., 2002). In addition, hepatic lipid accumulation could be resulted from imbalance between lipid acquisition and lipid disposal by an increased lipolysis or an increased fat intake, followed by the enhancement of free fatty acids (FFA). Plasma FFA, an important source for the TG synthesis in the liver, usually generated by white adipocytes via lipolysis can be taken up by FATP, caveolins, FAT/CD36, and FABP (Koo, 2013). FATP5 knockout (KO) mice showed the accumulation of hepatic triglycerides (TG) (Doege et al., 2006) whereas caveolin-1 KO mice exhibited lower hepatic TG accumulation (Fernandez et al., 2006). Moreover, in patients with NAFLD, increased level of hepatic FABP4 and FABP5 was observed and closely correlated with degree of hepatic fatty infiltration and percentage of liver fat (Westerbacka et al., 2007). Stimulation of DNL could contribute to fat accumulation in fatty liver. DNL starts with the conversion of acetyl-CoA to malonyl-CoA by acetyl-CoA carboxylase. Two regulatory transcription factors, sterol regulatory element-binding protein (SREBP)1c and carbohydrate regulatory element-binding protein (ChREBP) (Strable and Ntambi, 2010), are involved in the

[1]Department of Biological Sciences, College of Natural Sciences, Wonkwang University, Iksan, Jeonbuk 54538, Republic of Korea

[2]Integrated Omics Institute, Wonkwang University, Iksan, Jeonbuk 54538, Republic of Korea

[3]Asan Institute for Life Sciences, University of Ulsan College of Medicine, Seoul 05505, Republic of Korea

[4]Department of Pharmacy, College of Pharmacy, Wonkwang University, Iksan, Jeonbuk 54538, Republic of Korea

[5]Department of Internal Medicine, School of Medicine, Institute for Medical Science, Keimyung University, Daegu 42601, Korea

[6]Department of Pathology, Keimyung University School of Medicine, Daegu 42601, Korea

[7]Lead contact

*Correspondence: jineunjung@wku.ac.kr

https://doi.org/10.1016/j.isci.2022.105135

regulation of hepatic lipogenesis. SREBPs are responsible for activating almost 30 genes involved in lipid metabolism and resulted in the stimulation of DNL in hepatocytes (Shimano and Sato, 2017).

Fatty acid oxidation (FAO) significantly contributes to systemic lipid utilization and elevated level of FAO would increase oxidative capacity and lipid catabolism, reduce lipid load, and prevent the steatosis and lipotoxicity (Neuschwander-Tetri, 2010). FAs are oxidized primarily by mitochondrial and peroxisomal β-oxidation that catalyze the chain shortening of acyl-CoA (Hashimoto et al., 1999). As long-chain fatty acids cannot pass through the organelle membranes by simple diffusion, fatty acids have to be actively transported across both peroxisomal and mitochondrial membranes (Demarquoy and Le Borgne, 2015). Prior to transport, fatty acids are activated outside the organelles by conjugation to either coenzyme A (peroxisomes) or carnitine (mitochondria) (Schrader et al., 2015). Transport of acyl-CoA into the mitochondria is dependent on carnitine palmitoyltransferase-1 (CPT1) in the outer mitochondrial membranes and acyl-carnitines are transported across the inner mitochondrial membrane by CPT2 (Sharma and Black, 2009). Uncoupling of oxidation and phosphorylation in the mitochondria could induce the production of inflammatory cytokines and fibrogenic responses that are closely related to the development of fatty liver (Rolo et al., 2012). Unlike mitochondria that catalyze the β-oxidation of the short-, medium-, and long-chain fatty acids (LCFA), peroxisomes catalyze the β-oxidation of LCFAs and very long-chain fatty acids (VLCFAs) (Rolo et al., 2012). LCFAs and VLCFAs are oxidized in the peroxisomes to shortened fatty acids and transported into the mitochondria to be fully oxidized (Demarquoy and Le Borgne, 2015). Acyl-coenzyme A oxidase (ACOX1), a rate-limiting enzyme that is responsible for catabolism of VLCFAs in peroxisome, is related to the progression of fatty liver by regulating hepatic inflammation (Moreno-Fernandez et al., 2018). Acox1 deficiency in human fibroblasts significantly alters the inflammatory response, leading to the activation of the interleukin (IL)-1 pathway and the induction of IL-6 and IL-8 cytokines (El Hajj et al., 2012) suggesting that dysfunction of peroxisomal function might play an important role in the pathogenesis of fatty liver (Moreno-Fernandez et al., 2018). However, the functional role and underlying regulatory mechanism of peroxisome during the pathogenesis of fatty liver have not yet been well established.

In this study, we evaluated the important role of peroxisome in the pathogenesis of NAFLD and found that deficiency of peroxisomal nudix hydrolase 7 (NUDT7) is responsible for hepatic lipid accumulation and inflammatory responses through and the activation of hepatic DNL via activation of peroxisome proliferator-activated receptor (PPAR)γ. Moreover, we found that liraglutide, the most studied agent as a potential treatment option in NAFLD, reduced NAFLD induced by NUDT7 deficiency.

RESULTS

Peroxisomal dysfunction may be responsible for the pathogenesis of fatty liver

To identify the responsible factor and regulatory mechanism in hepatic steatosis, we applied in silico analysis with GSE33814 (20 steatosis patient liver tissues vs. 13 normal patient liver tissues) and GSE39549 (high-fat diet (HFD) mouse liver vs. normal chow diet (NCD) mouse liver). Gene set enrichment analysis (GSEA) suggested that the impaired peroxisome homeostasis might be responsible for the development of fatty liver (Figure 1A).

To verify the significance of peroxisomal function in the development and progression of fatty liver, lentivirus containing shRNA specific to *Acox1* (*shAcox1*), a peroxisomal β-oxidation initiation factor, was infected into C57BL/6 mice. Exposure of *shACOX1* into NCD mouse significantly increased hepatic TG, FFA, lipid accumulation, and lipid reactive oxygen species (ROS) without altering body and liver weight (Figures S1A and S1B). The transcription levels of genes involved in lipid metabolism, such as *Acaca*, *Cd36*, *Fasn*, *Fabp4*, and *Scd1*, were dramatically increased in the liver of *shAcox1*-infected (*shACOX1*) NCD mouse (Figure S1C). The expression levels of FASN, PPARγ, and SCD1 were dramatically increased in *shACOX1*-infected liver compared to control (*shCON*) liver (Figure S1D). In addition, catalase knockout (*Cat^{−/−}*) liver displayed the significantly increased levels of hepatic lipid accumulation (Figure S1E) with the increased the expression level of genes in lipid metabolism such as *Acaca*, *Cd36*, *Fasn*, *Fabp4*, and *Scd1* compared to *Cat^{+/+}* liver (Figure S1F).

Peroxisomal NUDT7 deficiency stimulates lipid accumulation in liver

In silico analysis of the expression of peroxisome-specific 193 probes using HFD mouse liver and NCD mouse liver showed that *NUDT7* was one of the most dramatically decreased in HFD mouse liver compared to NCD mouse liver (Figure 1B). Consistent with in silico analysis of GSE39549, we observed the increased expression level of *Nudt7* in HFD mouse liver compared to NCD mouse liver (Figure 1C). We analyzed the
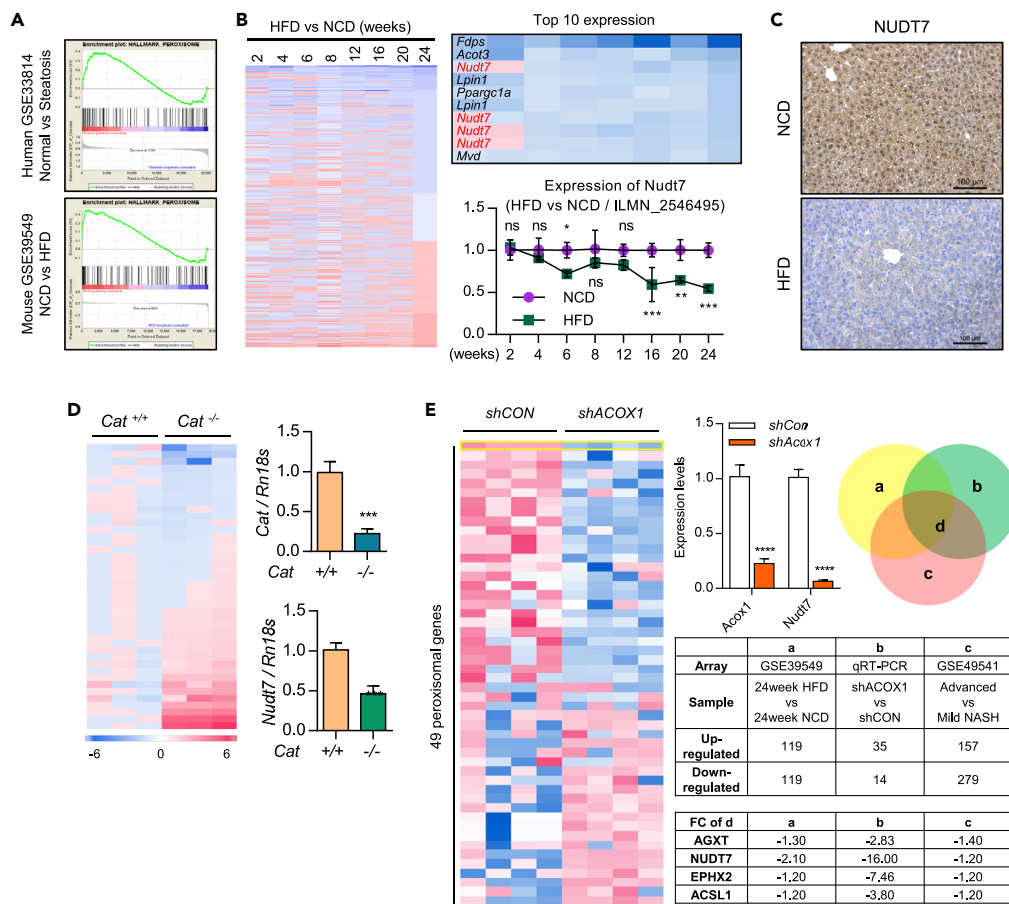
Figure 1. Peroxisome dysfunction may play an important role in the fatty liver

(A) Gene set analysis of GSE33814 (19 steatosis patient liver tissues vs. 13 normal patient liver tissues) and GSE39549 (3 HFD mouse liver vs. 3 NCD mouse liver).

(B) Analysis of peroxisomal genes in GSE39549 (liver of HFD mice vs. NCD mice) and the expression level of *Nudt7* in GSE39549 (n = 3).

(C) Representative images of NUDT7 staining in HFD liver compared to NCD liver (n = 4). Scale bars, 100 μm.

(D) Expression level of peroxisomal genes of $Cat^{+/+}$ and $Cat^{-/-}$ mouse liver using qRT-PCR (n = 3).

(E) Expression level of peroxisomal genes with *shCon* or *shAcox1* lentivirus-injected mouse liver using qRT-PCR (n = 4) and analyzed of peroxisomal genes in GSE39549 and GSE49541. Values were expressed as means + SD An unpaired *t*-test was used for statistical analysis. ns = non-significant, *p ≤ 0.05, **p < 0.01, ***p < 0.001.

expression levels of 42 peroxisome-specific genes using $Cat^{-/-}$ mouse liver and *Nudt7* was one of the most dramatically decreased peroxisomal genes in $Cat^{-/-}$ mouse liver (Figure 1D). In addition, among 49 peroxisome-specific genes tested, *Nudt7* was one of the most dramatically decreased genes in *shACOX1*-infected mouse liver compared to *shCON* mouse liver (Figure 1E).

We examined the expression level of NUDT7 in nonalcoholic fatty liver (NAFL) patient biopsy (Figure 2). Liver biopsy was collected from 27 patients who underwent bariatric and metabolic surgery. Among them, 5 patients without hepatic steatosis were excluded and 22 patients were enrolled. Histology of all of them showed NASH. Baseline characteristics are Table S1. Similar to in silico analysis, NUDT7 expression of liver tissue of patients with NASH was lower than that of normal subjects (Figures 2A and 2B). Patients with NASH were divided into two groups depending on the expression level of NUDT7 (Figures 2C and 2D). NAFLD activity-score (NAS) of patients with NASH with the low expression level of NUDT7 (n = 12) tends to be higher than those with a high expression level of NUDT7 (n = 10) (Figure 2C).

To investigate the role of *Nudt7* in the pathogenesis of hepatic steatosis, mouse primary hepatocytes were infected with shRNA specific for *Nudt7* (shNudt7). In *shNudt7*-infected hepatocytes, the levels of
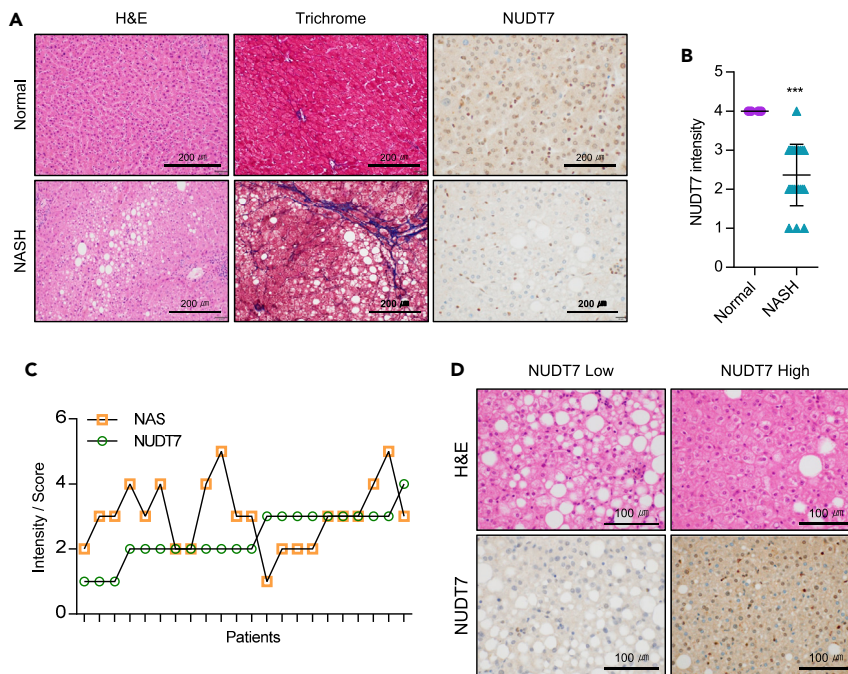
Figure 2. NUDT7 expression is suppressed in patients with NASH

(A) Representative images of H&E, trichrome, and NUDT7 in normal and NASH patients liver biopsy. Scale bars, 200 μm.

(B) NUDT7 staining intensity (4 normal vs. 22 NASH patient liver).

(C) Individual staining intensity of NUDT7 and NAS score in NASH patient liver.

(D) Representative H&E staining images depend on the expression level of NUDT7. Scale bars, 100 μm. ***p < 0.001 (Unpaired t-test).

LD, FFA,TG, free-, and ester-cholesterol were increased whereas activity of catalase was decreased (Figures S2A and S2B). The expression levels of genes in fatty acid accumulation such as *Acaca, Cd36, Fasn, Pparg,* and *Scd1* were also increased by the knockdown of *Nudt7* (Figure S2C). These increased levels of LD, FFA, TG, free-, and ester-cholesterol and increased levels of genes in fatty acid accumulation by the suppression of *Nudt7* were recovered by the restoration of *Nudt7*. As well, decreased level of catalase activity was recovered by the restoration of *Nudt7* (Figures S2A–S2C).

Heterozygous *Nudt7*^{+/−} mice develop fatty liver along with adipose expansion

For further investigation of NUDT7 involvement of in the pathogenesis of fatty liver, we applied NUDT7 knockout (KO) mice previously reported from our laboratory (Song et al., 2018). The expression level of NUDT7 was confirmed with liver of wild, homozygous *Nudt7* null (*Nudt7*^{−/−}), and heterozygous *Nudt7* null (*Nudt7*^{+/−}) NCD mice (Figure S3A). Consistent with our report with chondrocyte, we also observed the dysregulation of mitochondrial genes in *Nudt7*^{+/−} hepatocytes (Figure S3B). Significant increases in the weight of body and liver, the accumulation of lipid, and levels of serum AST, ALT, FFA, and hepatic TG were observed in *Nudt7*^{−/−} NCD liver (Figure S3C). Interestingly, *Nudt7*^{+/−} NCD mice become obese compared to wild-type (*Nudt7*^{+/+}) NCD mice (Figures 3A and S4). Body weight and liver-to-body weight ratio (Figure 3B), epididymal white adipose tissue (eWAT), and total WAT-to-body weight ratio (Figure S4A) were significantly increased in *Nudt7*^{+/−} NCD mice compared to *Nudt7*^{+/+} NCD mice. The accumulation of lipid droplets (LD) (Figure 3A), blood glucose, serum AST, ALT, hepatic FFA, and TG level was significantly increased in *Nudt7*^{+/−} NCD mice compared to *Nudt7*^{+/+} NCD mice (Figure 3C) without alterations of food and water intake (Figure 3B). Furthermore, O_2 consumption, CO_2 production, and night heat production were significantly decreased in *Nudt7*^{+/−} mice compared to *Nudt7*^{+/+} mice (Figure 3D). We observed the downregulation of *Nudt7* expression in GSE39549 of HFD mouse eWAT compared to NCD mouse eWAT (Figure S4B). Moreover, adipocyte size and the number of peroxisome membrane protein 70 (PMP70)-positive cells were also significantly increased in *Nudt7*^{+/−} adipose tissue (Figure S4C). Moreover, the expression levels of lipogenic genes such as *Fasn, Scd1, Acaca, Cidea, Srebf2,* and *Fabp4,* lipid metabolism such as *Abca1, Prkaa1, Irs2, Crot, Sirt6,* and *Chrebf,* adipokines such as *Il1b, Il6, Tnfa, Ccl2, Ccl4, Cxcl2, Lep,* and *Lcn2,* and lipolysis genes such as *Atgl, Mgl,* and *Hsl*
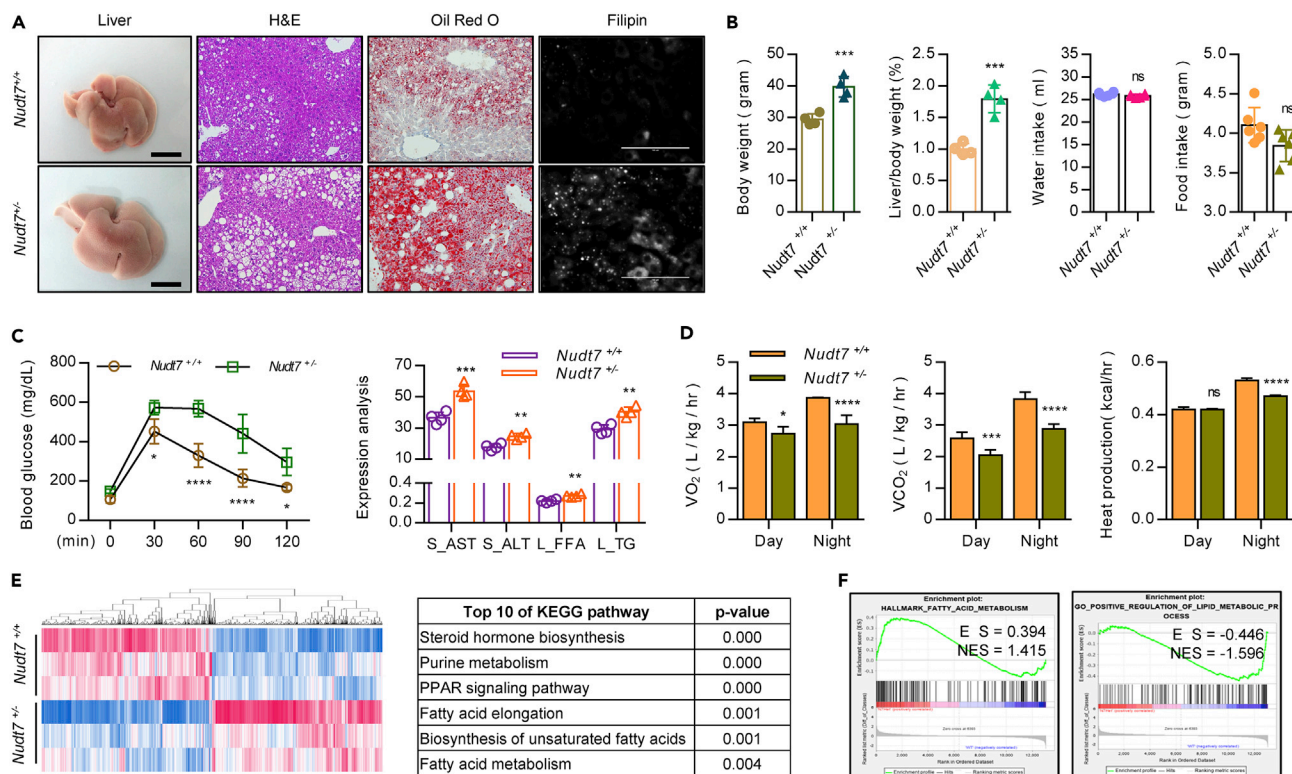
Figure 3. *Nudt7+/−* mice display typical characteristics of fatty liver

(A) Representative images of liver, H&E, Oil Red O, and Filipin staining in *Nudt7+/+* and *Nudt7+/−* mouse liver (n = 4).

(B) Food and water intake (n = 6), body and liver per body weight (n = 4).

(C) Analysis of blood glucose level (left panel) in *Nudt7+/+* (n = 4) and *Nudt7+/−* (n = 4) mouse and serum AST and ALT, hepatic FFA and TG level (n = 4).

(D) Oxygen consumption (VO$_2$), CO$_2$ production (VCO$_2$), and heat production were analyzed (n = 5).

(E) RNA sequencing data of 12-month-old *Nudt7+/+* and *Nudt7+/−* liver were analyzed using KEGG pathway enrichment analysis (n = 3).

(F) Gene set analysis of *Nudt7+/+* and *Nudt7+/−* mouse liver. ns = non-significant, *p ≤ 0.05, **p < 0.01, ***p < 0.001, ****p < 0.0001 (Unpaired t-test or two-way ANOVA).

(Figure S4D) were significantly increased in *Nudt7+/−* adipocyte compared to *Nudt7+/+* adipocyte. The expression level of lipid transport genes such as *Abca1, Abcg1, Apoa,* and *Apob* was also significantly increased in in *Nudt7+/−* adipocyte (Figure S4E). Increased in the hypertrophy and expression level of adipokine genes, *Lep* and *Lcn2* were significantly suppressed by the restoration of NUDT7 in *Nudt7+/−* adipocytes (Figure S4F). To confirm the possible involvement of adipose tissue in *Nudt7+/−*-induced NAFLD, primary hepatocyte of *Nudt7+/+* and *Nudt7+/−* mice was co-cultured with either adipocyte of *Nudt7+/+* or *Nudt7+/−* mice (Figure S5A). Lipid accumulation and expression levels of *Fasn, MLL3,* and *Srebf1* were significantly upregulated in hepatocyte of *Nudt7+/+* or *Nudt7+/−* mice co-cultured with adipocytes of *Nudt7+/−* mice (Figure S5B).

Heterozygous *Nudt7+/−* mice develop fatty liver via activation of PPAR signaling

For further understanding of biological and signaling mechanism underlying NUDT7 deficiency-induced fatty liver, RNA sequencing was performed on RNA isolated from 12-month-old *Nudt7+/+* and *Nudt7+/−* liver. Analysis of RNA sequencing showed 1,558 genes with fold change more than 1.5 (779 upregulated genes and 779 downregulated genes), whose expressions were significant differ between *Nudt7+/+* and *Nudt7+/−* liver (Figure 3E). KEGG analysis suggested the PPAR signaling as one of the enriched signaling pathways in *Nudt7+/−* mouse liver (Figure 3E). Moreover, fatty acid metabolism and lipid metabolic process were significantly increased in *Nudt7+/−* liver (Figure 3F).

Histological analysis showed the increased level of PPARγ in *Nudt7+/−* mouse liver (Figures 4A and 4B). In addition, the expression levels of PPARγ target genes such as *Cd36, Fabp4,* and *Il6* were significantly increased in *Nudt7+/−* liver (Figure 4C). To investigate the biological functional role of PPARγ in *Nudt7+/−* liver, genes known to interact with PPARγ were extracted from RNA sequencing and subjected
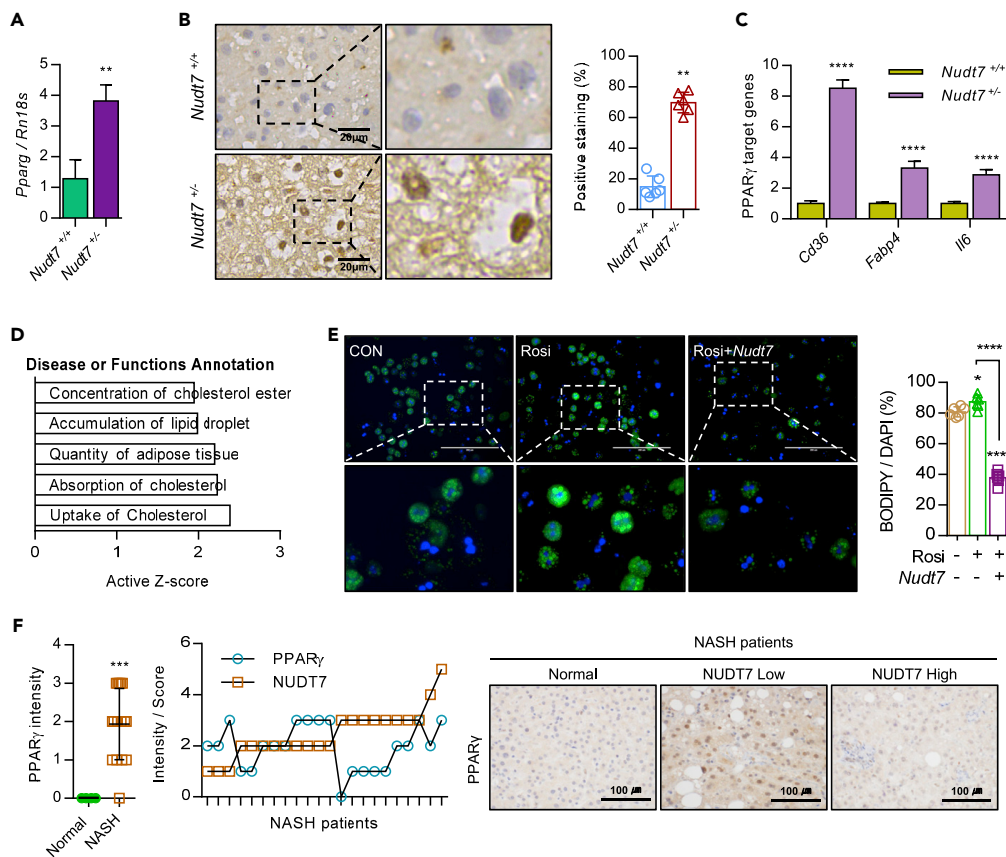
Figure 4. Activation of PPARγ in *Nudt7*^{+/−} liver is responsible for hepatic lipid accumulation

(A) The expression level of *Pparg* in *Nudt7*^{+/+} and *Nudt7*^{+/−} mouse liver was analyzed using qRT-PCR.

(B) Representative image of PPARγ in 12-month-old *Nudt7*^{+/−} liver compared to *Nudt7*^{+/+} liver (n = 3; Scale bars, 20 μm) and positive staining ratio (n = 6 per group).

(C) The expression levels of PPARγ target genes (*Cd36*, *Fabp4*, and *Il6*) were analyzed by qRT-PCR (n = 3).

(D) Genes related to PPARγ signaling were extracted from the RNA sequencing data (n = 3) and subjected to IPA.

(E) Representative images of BODIPY[493/508] staining and positive cell counting (n = 6 per group) in primary cultures of *Nudt7*^{+/−} hepatocytes in the presence of 10 μM rosiglitazone (Rosi) with pcDNA-*Nudt7* for 24 h. Scale bars, 200 μm.

(F) Representative images and intensity of PPARγ in NASH liver (n = 22) compared to normal liver (n = 4) biopsy. Scale bars, 100 μm. *$p \leq 0.05$, **$p < 0.01$, ***$p < 0.001$, ****$p < 0.0001$ (Unpaired t-test or onw-way ANOVA).

to IPA (Figure 4D). IPA revealed that these PPARγ-interacting genes were involved in lipid metabolism and cholesterol uptake and absorption (Figure 4D). Exposure of rosiglitazone (Rosi), a known to PPARγ agonist, into primary hepatocytes of *Nudt7*^{+/+}or *Nudt7*^{+/−} mouse, significantly induced the LD accumulation and this increased LD accumulation was reduced by co-introduction of *Nudt7* (Figures 4E and S6). In patients with NASH divided by the expression level of NUDT7 (high vs. low), we observed a significant increase of PPARγ in patients with NASH with low expression level of NUDT7 compared to patients with high expression of NUDT7 (Figure 4F).

Palmitic acid accumulated by NUDT7 deficiency stimulates H3K4me3 on *Pparg* promoter

To investigate the involvement of epigenetic regulation of NUDT7 deficiency in *Pparg*, we analyzed the methylation status of *Pparg* promoter. We observed a significant increase level of histone H3K4me3 in *Nudt7*^{+/−} liver compared to *Nudt7*^{+/+} liver (Figure 5A). Moreover, the expression level of histone lysine methyltransferase (MLL) family member, particularly *Mll3* and *Mll4* known as H3K4 methyltransferase family member (Hu et al., 2013), was significantly increased in *Nudt7*^{+/−} liver (Figure 5B). Nuclear staining of H3K4me3 was significantly increased in liver of *Nudt7*^{+/−} mouse compared to *Nudt7*^{+/+} mouse (Figure 5C). Expression levels of DNA methyltransferases (DNMTs) known to inhibit H3K4me3 (Rose and Klose, 2014) such as *Dnmt3b*, *Dnmt3l*, and *Mecp2* were significantly decreased in *Nudt7*^{+/−} liver (Figure S7A).
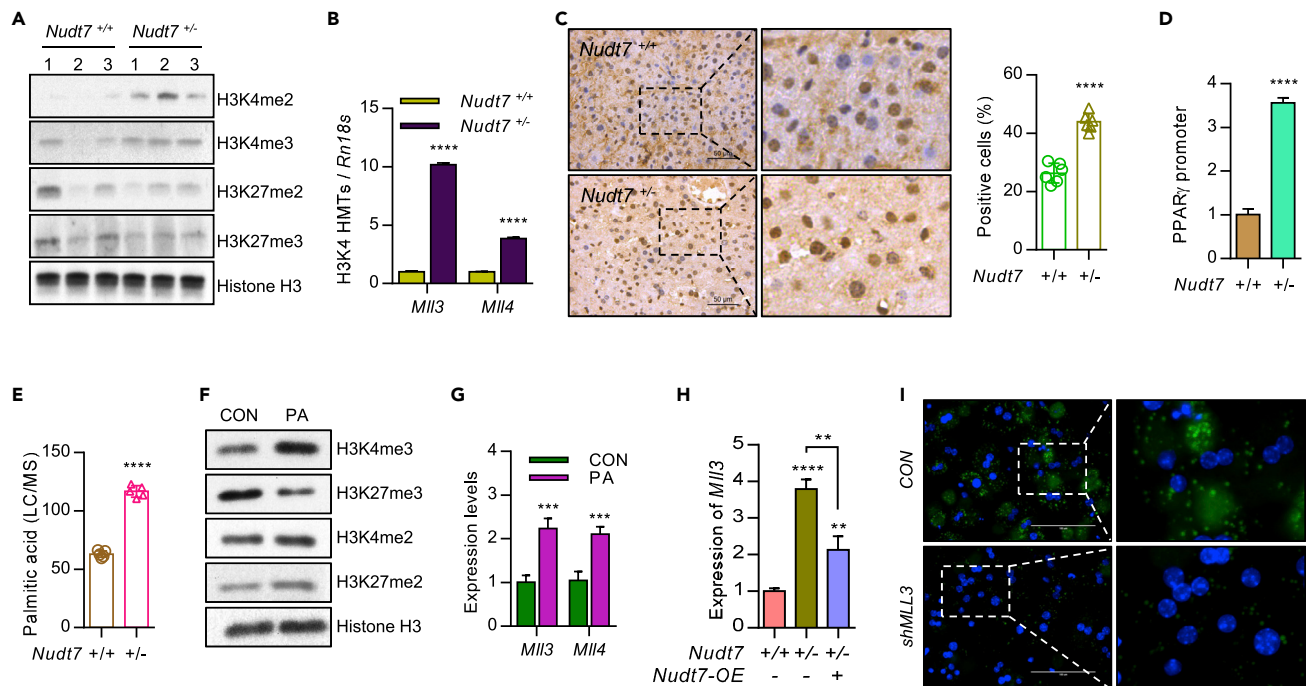
Figure 5. Accumulated palmitic acid in Nudt7^{+/−} liver is responsible for PPARγ activation

(A) The methylation levels of H3K4me2, H3K4me3, H3K27me2, and H3K27me3 were analyzed by immunoblotting in Nudt7^{+/+} and Nudt7^{+/−} liver. Histone H3 was used for loading control (n = 3).

(B) The transcription levels of Mll3 and Mll4 were analyzed by qRT-PCR (n = 3).

(C) Representative images of H3K4me3 staining in the 12-month-old mouse liver (n = 3; Scale bars, 50 μm) and positive staining ratio (n = 6 per group).

(D) H3K4me3 level on PPARγ promoter was analyzed using qRT-PCR. DNA was isolated using chromatin immunoprecipitation (ChIP) in Nudt7^{+/+} and Nudt7^{+/−} liver (n = 3).

(E) Palmitic acid level in Nudt7^{+/+} and Nudt7^{+/−} liver (n = 5).

(F) Primary cultures of Nudt7^{+/+} hepatocytes were treated with BSA-conjugated with 50 μM palmitic acid (PA) or BSA alone (CON) and the expression level of H3K4me3, H3K27me3, H3K4me2, and H3K27me2 were analyzed by immunoblotting. Histone H3 was used for loading control.

(G) The expression levels of Mll3 and Mll4 were analyzed by qRT-PCR (n = 3).

(H) Primary cultures of Nudt7^{+/+} and Nudt7^{+/−} hepatocytes were infected with lentiviruses containing NUDT7 (Nudt7-OE, +) or mock control (−) and the expression level of Mll3 was analyzed by qRT-PCR (n = 3).

(I) Representative images of BODIPY^{493/508} staining in primary cultures of Nudt7^{+/−} hepatocytes transduced with shMll3 for 24 h. Scale bars, 100 μm.

*p ≤ 0.05, **p < 0.01, ***p < 0.001, ****p < 0.0001 (Unpaired t-test or one-way ANOVA).

Exposure of DNA methylation inhibitors such as trichostatin A (TSA; 5 mM) or 5-Aza-2'-deoxycytidine (5-aza; 10 mM) into primary mouse hepatocytes induced the expression of Mll3 (Figure S7B) as well as the expression level of DNL genes (Figure S7C). Chromatin immunoprecipitation (ChIP) qRT-PCR assay showed that H3K4me3 on Pparg promoter was significantly increased in Nudt7^{+/−} liver compared with Nudt7^{+/+} liver (Figure 5D).

Lipid analysis showed that palmitic acid (C16:0, PA) was the most significantly increased FA in Nudt7^{+/−} mouse (Figures 5E and S7D) and exposure of PA into primary hepatocytes induced the expression level of H3K4me3 (Figure 5F) as well as the expression levels of Mll3 and Mll4 (Figure 5G). Increased level of Mll3 in Nudt7^{+/−} hepatocytes was reduced by Nudt7 restoration (Figure 5H). Increased level of lipid accumulation (Figure 5I) and inflammatory cytokines in Nudt7^{+/−} hepatocytes was also significantly decreased by Mll3 knockdown (Figure S7E). Restoration of Nudt7 into Nudt7^{+/−} mouse significantly decreased glucose and insulin tolerance (Figure S8) and the accumulation of LD in Nudt7^{+/−} mouse liver (Figure 6A). The number of H3K4me3- and PPARγ-positive cells (Figure 6A), the levels of serum AST, ALT, FFA, and hepatic cholesterol (Figure 6B), expression level of PPARγ-downstream genes (Figure 6C), Mll3, Mll4, and chemokine genes (Figure 6D) were significantly decreased by the restoration of Nudt7. Moreover, restoration of Nudt7 reduced adipocyte size and the number of PMP70-positive cells in Nudt7^{+/−} adipose tissue (Figure 6E).
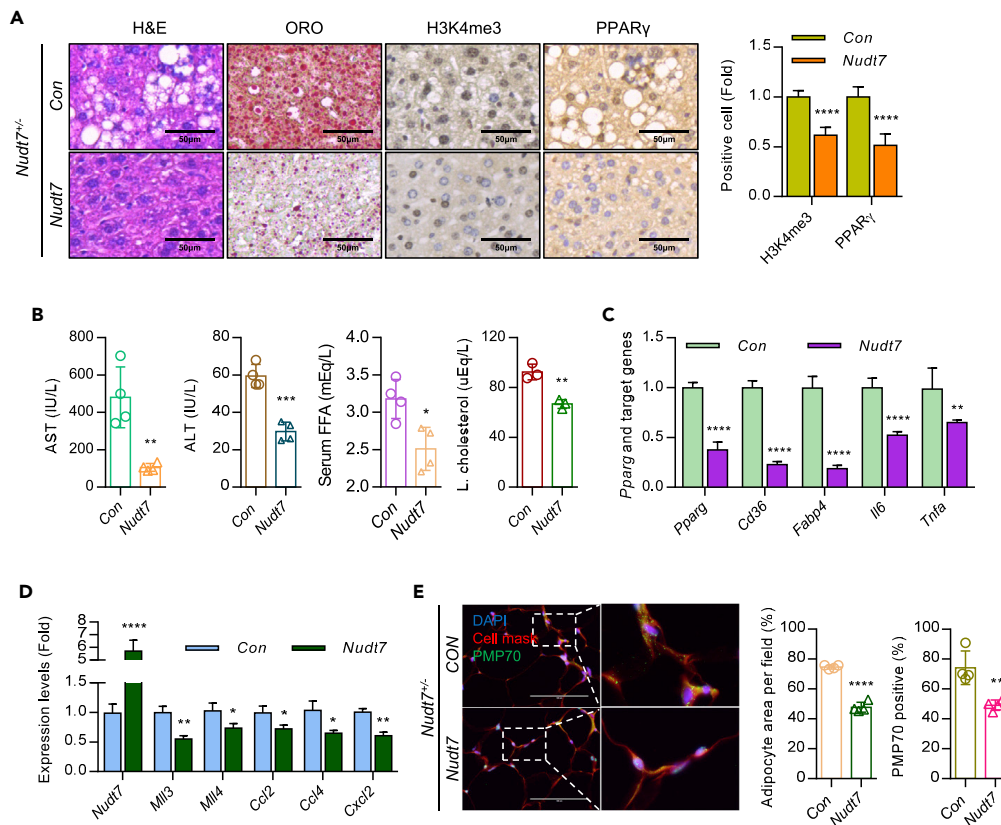
Figure 6. Restoration of *Nudt7* reduces hepatic lipid accumulation, H3K4me3 of PPARγ, and inflammatory responses

(A) *Nudt7^{+/−}* mice were tail-vein injected with lentiviruses containing *Nudt7* or mock control (CON). Representative images of H&E and ORO staining and immunohistochemistry images of H3K4me3 and PPARγ staining (n = 3). Bar graph of H3K4me3 and PPARγ positive staining intensity was represented as the fold of CON (n = 6).

(B) The levels of serum AST, ALT, FFA, and hepatic cholesterol were analyzed (n = 4).

(C) The expression level of *Pparg*, *Cd36*, *Fabp4*, *Il6*, and *Tnfa* was analyzed using qRT-PCR (n = 3).

(D) The expression level of *Nudt7*, *Mll3*, *Mll4*, *Ccl2*, *Ccl4*, and *Cxcl2* was analyzed using qRT-PCR (n = 3).

(E) Representative images of cell mask orange and PMP70 staining and graphs with adipocyte area per filed and percentage of PMP70-positive cell counting (n = 4; Scale bars, 100 μm). *p ≤ 0.05, **p < 0.01, **p < 0.01, ***p < 0.001, ****p < 0.0001 (Unpaired t-test).

Liraglutide attenuates hepatic lipid accumulation and hepatic DNL induced by NUDT7 deficiency

Liraglutide, the widely used glucagon-like peptide-1 receptor agonist (GLP-1 RA), known as an intrinsic PPARγ activator in endothelial cells (Onuma et al., 2014), is an agent considering as potent treatment option for NAFLD. The GLP-1 RA enhances intrinsic PPARγ activity. However, the mechanism of liraglutide underlying NAFLD is not well studied. In this study, to investigate whether liraglutide reduces the fatty liver induced by NUDT7 deficiency, we administrated 200 μg/kg body weight liraglutide into *Nudt7^{+/−}* and *Nudt7^{+/−}* mouse intraperitoneally. Interestingly, the expression level of NUDT7 was significantly increased in liraglutide-administrated *Nudt7^{+/+}* liver (Figure 7A). Furthermore, the expression level of PPARγ and H3K4me3 was significantly decreased in liraglutide-administrated *Nudt7^{+/+}* liver (Figure 7A). Administration of liraglutide significantly decreased the weight of body and liver (Figures S9A–S9C) as well as lipid accumulation (Figure 7B) in HFD *Nudt7^{+/−}* mouse. Significantly reduced level of hepatic FFA, TG, and cholesterol accumulation (Figure 7C), FABP4, SCD1, PPARγ, and H3K4me3 (Figure 7D), and the expression level of gene in lipogenesis, lipid metabolism, and cytokine (Figure 7E) was observed in liraglutide-administrated *Nudt7^{+/−}* liver.

To rule out the possible involvement of adipose tissue in the action of liraglutide with *Nudt7^{+/−}* mouse and verify the role of liraglutide in hepatocytes, we isolated hepatocyte from *Nudt7^{+/−}* mouse and cultured with or without
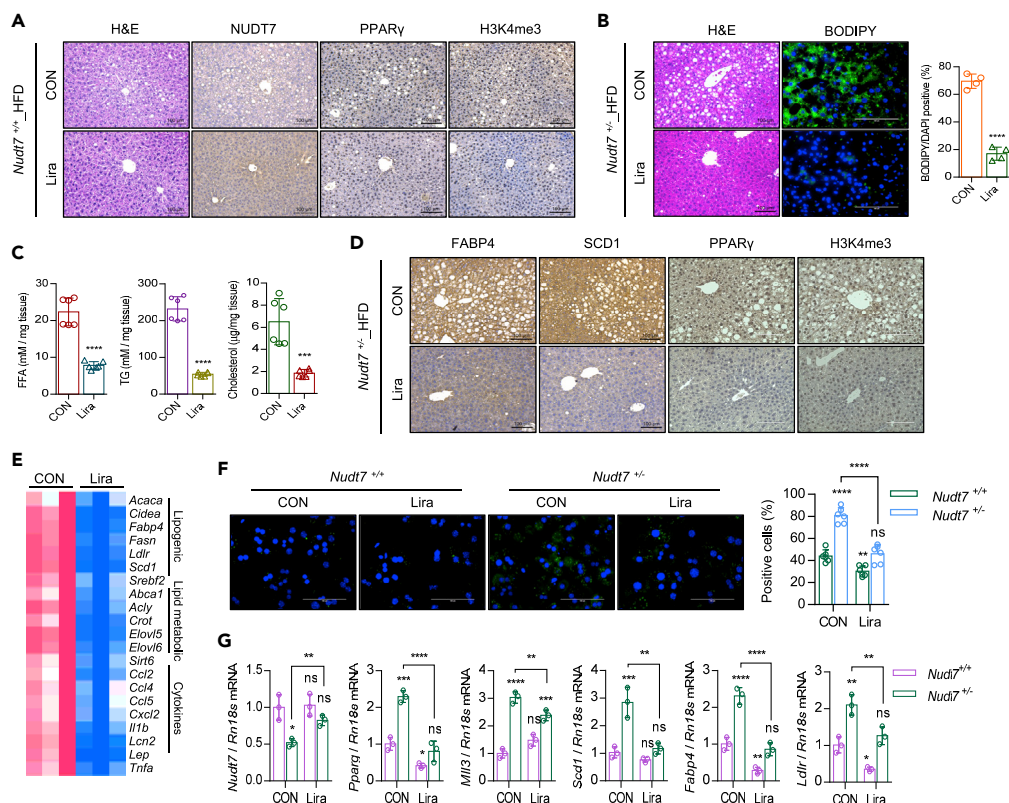
Figure 7. Liraglutide suppresses fatty liver induced by *Nudt7* deficiency

(A) Representative images of H&E, NUDT7, PPARγ, and H3K4me3 in mouse liver of HFD-fed *Nudt7*^{+/+} mice with liraglutide or equal volume of sterile saline i.p. injected mouse.

(B) Representative image of H&E and BODIPY staining and the number of BODIPY positive cells in HFD-fed *Nudt7*^{+/−} mice with liraglutide or equal volume of sterile saline i.p. injected mouse. (n = 4; Scale bar, 100 μm).

(C) Hepatic FFA, TG, and cholesterol were analyzed in HFD-fed *Nudt7*^{+/−} mice liver (n = 6).

(D) Representative images of FABP4, SCD1, PPARγ, and H3K4me3 staining (n = 3; Scale bars, 100 μm).

(E) The expression level of lipogenic, lipid metabolism, and cytokine genes was analyzed using qRT-PCR (n = 3).

(F) Representative image of BODIPY staining and the number of BODIPY positive cells in primary hepatocyte with or without 100 nM liraglutide (n = 6; Scale bars, 100 μm).

(G) The expression level of Nudt7, Pparg, Mll3, Scd1, Fabp4, and Ldlr was analyzed using qRT-PCR (n = 3). $**p < 0.01$, $***p < 0.001$, $****p < 0.0001$ (Unpaired t-test).

100 nM liraglutide (Figure 7F). In primary cultured *Nudt7*^{+/−} hepatocyte, lipid accumulation was significantly suppressed with treatment of liraglutide (Figure 7F) along with a significant increase in the expression level of *Nudt7* and significant decrease in the expression level of *Pparg, Mll3, Scd1, Fabp4, and Ldlr* (Figure 7G).

DISCUSSION

Even though increasing evidences suggested that peroxisomes that closely interact with mitochondria might be one of the key regulatory organelles in lipid metabolism (Demarquoy and Le Borgne, 2015) and peroxisomal function may play an important role in hepatic lipid metabolism (Lodhi and Semenkovich, 2014), only a few studies have been demonstrated the importance of peroxisomal function in the accumulation of hepatic lipid droplets (LD). Recently, it has been suggested that dysregulation of organelle interaction between peroxisome and mitochondria may be responsible for the development of fatty liver disease by abnormal regulation of fatty acid β-oxidation (Shai et al., 2016). Moreno-Fernandez and colleagues (2018) reported that the depletion of *Acox1* caused hepatic lipid accumulation and inflammation (Moreno-Fernandez et al., 20182018). Consistent with this, our IPA using GEO dataset of advanced and mild nonalcoholic steatohepatitis (NASH) indicated that peroxisomal function, particularly fatty acid β-oxidation was significantly decreased in the advanced NASH compared to mild NASH. Among peroxisomal genes, we observed that peroxisomal nudix hydrolase 7 (*Nudt7*), one of family members of CoA diphosphatase mediating the cleavage of CoA, CoA

esters, and oxidized CoA (Gasmi and McLennan, 2001), is significantly decreased in the primary hepatocytes isolated from $Cat^{-/-}$ mouse and HFD-induced mouse. $Nudt7^{+/-}$ mice displayed the typical characteristics of fatty liver $i.e.$ increased levels of FFA, AST, ALT, and hepatic triglyceride (TG). Furthermore, decreased level of peroxisomal $Nudt7$ is responsible for the stimulation of inflammatory responses leading to the stimulation of inflammatory cytokines such as IL-1β, IL-6, and TNFα. These suggest that peroxisomal dysfunction via the suppression of $Nudt7$ may play an important role in the pathogenesis of fatty liver. Profound changes in adipose tissue are closely associated with the pathogenesis of fatty liver (Tamura and Shimomura, 2005). Adipocytes, the functional unit of adipose tissue performed the central role of lipid uptake and storage and releasing excess energy in the form of TG and FFA (Rector et al., 2008). Impairing the ability to absorb and store fatty acid in adipocytes or increasing lipolysis from adipose tissue led to the increased flux of fatty acid to the liver and inflammation and fibrosis in the liver (Rector et al., 2008). Recent study (Park et al., 2019) suggested that the disruption of peroxisomal biogenesis impaired adipose tissue thermogenesis. Adipose-specific KO of $Pex16$, the critical factor for assembly of the peroxisomal membrane and import of peroxisomal membrane proteins, decreased energy expenditure and increased the diet-induced obesity. On the other hand, adipose-specific KO of peroxisomal β-oxidation enzyme $Acox1$ did not affect adiposity and thermogenesis. Here, in our study, $Nudt7^{+/-}$ mice displayed the impaired WAT remodeling capacity, $i.e.$ increased the lipolysis of adipose tissue suggesting that regulation of adipose tissue by NUDT7-induced secondary effects in the liver contributing to the development of NFALD. Interestingly, we observed the increased number of peroxisome in the adipose tissue of $Nudt7^{+/-}$ mice. We believe that this is due to a compensatory mechanism for peroxisomal dysfunction in $Nudt7^{+/-}$ mice, and research is currently ongoing to prove this. Moreover, since we found that co-culture of $Nudt7^{+/+}$ hepatocyte with $Nudt7^{+/-}$ adipocyte induces lipid accumulation and activation of lipogenic genes suggesting the interaction between hepatocyte and adipocyte in the development of NFALD in $Nudt7^{+/-}$ mice, detailed studies on interaction between hepatocyte and adipocyte are also ongoing.

Peroxisome proliferator-activated receptors (PPARs), member of the nuclear receptor superfamily (Raney et al., 1997), are known to regulate lipid synthesis, glucose metabolism, and cholesterol efflux in various cell types including hepatocytes, adipocytes, and macrophages. PPARγ, highly expressed in adipose tissue and macrophage, plays important roles in lipid metabolism such as fatty acid uptake, β-oxidation and TG turnover, insulin resistance, and immune regulation (Cave et al., 2016; Lee et al., 1995). Hepatocyte PPARγ has been known as a steatogenic factors while others suggest the activation of PPARγ reduces hepatic steatosis. Previously, it has been reported that overexpression of PPARγ leads to ectopic fat deposition in the liver (Gross et al., 2017). Increase level of PPARγ has been shown in steatotic liver of animal models or patients with NAFLD (Matsusue et al., 2003). Hepatocyte-specific PPARγ knockout was associated with a reduction in the expression level of DNL genes. HFD-induced hepatic steatosis and lipogenesis genes such as $Scd1$, $Srebf1c$, and Acc were significantly reduced in hepatocyte-specific PPARγ knockout mice (Moran-Salvador et al., 2011). However, other groups (Wolf Greenstein et al., 2017) reported that liver (hepatocyte)-specific PPARγ knockdown in HFD mouse reduced the accumulation of hepatic TG but not the expression of DNL genes suggesting that PPARγ plays a minimal role in directly regulating hepatic DNL. In this study, we found that $Nudt7$ deficiency induced the over-activation of PPARγ and stimulated the accumulation of hepatic TG and DNL. Moreover, we found that the level of H3K4me3 in the $Pparg$ promoter was significantly upregulated in the hepatocytes of $Nudt7^{+/-}$ liver due to increased level of an endogenous lipid that can activate PPARs, palmitic acid in $Nudt7^{+/-}$ liver. It has been reported that PPARs are activated by endogenous lipids such as free fatty acids (FFAs) and eicosanoids (Wahli and Michalik, 2012; Tailleux et al., 2012). Fatty acids such as palmitic acid, oleic acid, and prostaglandins have been identified as natural ligands for PPARs (Tailleux et al., 2012).

Since the controversial role of PPARγ on NALFD has been reported, the effect of rosiglitazone, a PPARγ agonist on improving or exacerbating NAFLD also contradictory [65, 66]. In HFD liver, treatment of rosiglitazone significantly increased in the accumulation of TG and lipid unlike to NCD liver (Gao et al., 2016). In A-ZIP/F-1 mouse, a model for the human disease lipoatrophic diabetes (Gavrilova et al., 2003), the treatment of rosiglitazone also significantly increased the accumulation of hepatic TG by the activation of PPARγ (Wahli and Michalik, 2012). In this study, we also found that exposure of rosiglitazone into $Nudt7^{+/-}$ hepatocytes accumulated LD and this lipid accumulation dramatically reduced the restoration of $Nudt7$. Recently, glucagon-like peptide-1 (GLP-1) receptors, known to express in hepatocytes, had been experimentally and clinically shown to ameliorate NAFLD (Lee et al., 2012). In liver biopsy specimens from patients with NASH, the number of GLP-1 receptors is reduced as well as in animal NAFLD models (Svegliati-Baroni et al., 2011). Liraglutide, the most widely used GLP-1 receptor agonists, is an attractive candidate for the treatment of
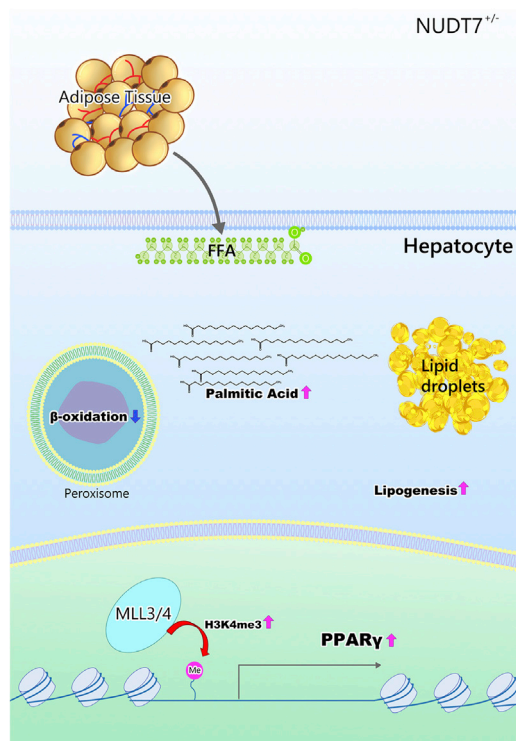
Figure 8. Diagram of the suggested mechanism by which deficiency of peroxisomal NUDT7 induces NAFLD

NAFLD shown with multiple preclinical studies and clinical trials (Lv et al., 2020). Recent experimental study suggests that liraglutide might decrease hepatic inflammation and hepatocyte ballooning (Ipsen et al., 2018; Kojima et al., 2020). Moreover, liraglutide is known to reverse oxidative stress by activating PPARα to inhibit the expression of diacylglycerolacyl O-acetyltransferase (DGAT) in diabetes (Zhang et al., 2018) and reduce hepatic fatty acid flux by decreasing PPAR-γ in the liver of diet-induced obesity rats (Decara et al., 2016). However, the relationship between the effects of liraglutide on regulating hepatic inflammation and lipid metabolism remains unclear. Here, we observed that liraglutide reverses the NAFLD features induced by NUDT7 deficiency by regulating NUDT7-PPARγ axis. In addition, we also found the elevated level of PPARα in *Nudt7*^{+/−} hepatocytes suggesting the possible role of PPARα in the pathogenesis of NAFLD induced by NUDT7 deficiency and the investigation on the role of other PPAR family including PPARα in NAFLD induced by NUDT7 deficiency is currently undergoing in our laboratory.

Taken together, here, peroxisomal *Nudt7* deficiency displayed fatty liver due to an increased hepatic DNL via activation of PPARγ through upregulation of H3K4me3 and this could be reversed by liraglutide (Figure 8). Because of the interplay between peroxisomes and mitochondria in maintaining lipid homeostasis, we would expect that the mitochondrial dysfunction may be associated with NAFLD induced by NUDT7 deficiency and remains to be investigated further.

Limitations of the study

Our study demonstrates that heterozygous deficiency of a peroxisomal gene, *Nudt7*, could be responsible for NAFLD through DNL-PPAR PPARγ activation and liraglutide markedly prevented NAFLD induced by NUDT7 deficiency. The limitation of this study is the number of patients used in this study. Further investigation with a large pool of patients to verify Nudt7 as biomarker and potent therapeutic and clinical application for NAFLD will be warranted.

STAR★METHODS

Detailed methods are provided in the online version of this paper and include the following:

- KEY RESOURCES TABLE
- RESOURCE AVAILABILITY

SUPPLEMENTAL INFORMATION

Supplemental information can be found online at https://doi.org/10.1016/j.isci.2022.105135.

AUTHOR CONTRIBUTIONS

Conceptualization: E-J.J.; Data curation: J.S. and K.S.; Formal analysis: J.S.; Funding acquisition: E-J.J. and J.S.; Investigation: J.S., I-J.B., S.P., J.O., D.K., M.K.K., H.W.L., and B.K.J.; Writing original draft: E-J.J.

DECLARATION OF INTERESTS

The authors declare that they have no competing interests.

REFERENCES

Benedict, M., and Zhang, X. (2017). Non-alcoholic fatty liver disease: an expanded review. World J. Hepatol. *9*, 715–732.

Cave, M.C., Clair, H.B., Hardesty, J.E., Falkner, K.C., Feng, W., Clark, B.J., Sidey, J., Shi, H., Aqel, B.A., McClain, C.J., and Prough, R.A. (2016). Nuclear receptors and nonalcoholic fatty liver disease. Biochim. Biophys. Acta *1859*, 1083–1099.

Chao, L., Marcus-Samuels, B., Mason, M.M., Moitra, J., Vinson, C., Arioglu, E., Gavrilova, O., and Reitman, M.L. (2000). Adipose tissue is required for the antidiabetic, but not for the hypolipidemic, effect of thiazolidinediones. J. Clin. Invest. *106*, 1221–1228.

Decara, J., Arrabal, S., Beiroa, D., Rivera, P., Vargas, A., Serrano, A., Pavón, F.J., Ballesteros, J., Dieguez, C., Nogueiras, R., et al. (2016). Antiobesity efficacy of GLP-1 receptor agonist liraglutide is associated with peripheral tissue-specific modulation of lipid metabolic regulators. Biofactors *42*, 600–611.

Demarquoy, J., and Le Borgne, F. (2015). Crosstalk between mitochondria and peroxisomes. World J. Biol. Chem. *6*, 301–309.

Doege, H., Baillie, R.A., Ortegon, A.M., Tsang, B., Wu, Q., Punreddy, S., Hirsch, D., Watson, N., Gimeno, R.E., and Stahl, A. (2006). Targeted deletion of FATP5 reveals multiple functions in liver metabolism: alterations in hepatic lipid homeostasis. Gastroenterology *130*, 1245–1258.

El Hajj, H.I., Vluggens, A., Andreoletti, P., Ragot, K., Mandard, S., Kersten, S., Waterham, H.R., Lizard, G., Wanders, R.J.A., Reddy, J.K., and Cherkaoui-Malki, M. (2012). The inflammatory response in acyl-CoA oxidase 1 deficiency (pseudoneonatal adrenoleukodystrophy). Endocrinology *153*, 2568–2575.

Fabbrini, E., Sullivan, S., and Klein, S. (2010). Obesity and nonalcoholic fatty liver disease: biochemical, metabolic, and clinical implications. Hepatology *51*, 679–689.

Farrell, G.C., and Larter, C.Z. (2006). Nonalcoholic fatty liver disease: from steatosis to cirrhosis. Hepatology *43*, S99–S112.

Fernandez, M.A., Albor, C., Ingelmo-Torres, M., Nixon, S.J., Ferguson, C., Kurzchalia, T., Tebar, F., Enrich, C., Parton, R.G., and Pol, A. (2006). Pol, Caveolin-1 is essential for liver regeneration. Science *313*, 1628–1632.

Gao, M., Ma, Y., Alsaggar, M., and Liu, D. (2016). Dual outcomes of rosiglitazone treatment on fatty liver. AAPS J. *18*, 1023–1031.

Gavrilova, O., Haluzik, M., Matsusue, K., Cutson, J.J., Johnson, L., Dietz, K.R., Nicol, C.J., Vinson, C., Gonzalez, F.J., and Reitman, M.L. (2003). Liver peroxisome proliferator-activated receptor gamma contributes to hepatic steatosis, triglyceride clearance, and regulation of body fat mass. J. Biol. Chem. *278*, 34268–34276.

Gong, Z., Tas, E., Yakar, S., and Muzumdar, R. (2017). Hepatic lipid metabolism and non-alcoholic fatty liver disease in aging. Mol. Cell. Endocrinol. *455*, 115–130.

Gross, B., Pawlak, M., Lefebvre, P., and Staels, B. (2017). PPARs in obesity-induced T2DM, dyslipidaemia and NAFLD. Nat. Rev. Endocrinol. *13*, 36–49.

Hashimoto, T., Fujita, T., Usuda, N., Cook, W., Qi, C., Peters, J.M., Gonzalez, F.J., Yeldandi, A.V., Rao, M.S., and Reddy, J.K. (1999). Peroxisomal and mitochondrial fatty acid beta-oxidation in mice nullizygous for both peroxisome proliferator-activated receptor alpha and peroxisomal fatty acyl-CoA oxidase. Genotype correlation with fatty liver phenotype. J. Biol. Chem. *274*, 19228–19236.

Hu, D., Gao, X., Morgan, M.A., Herz, H.M., Smith, E.R., and Shilatifard, A. (2013). The MLL3/MLL4 branches of the COMPASS family function as major histone H3K4 monomethylases at enhancers. Mol. Cell Biol. *33*, 4745–4754.

Hui, T.Y., Olivier, L.M., Kang, S., and Davis, R.A. (2002). Microsomal triglyceride transfer protein is essential for hepatic secretion of apoB-100 and apoB-48 but not triglyceride. J. Lipid Res. *43*, 785–793.

Ipsen, D.H., Rolin, B., Rakipovski, G., Skovsted, G.F., Madsen, A., Kolstrup, S., Schou-Pedersen, A.M., Skat-Rørdam, J., Lykkesfeldt, J., and Tveden-Nyborg, P. (2018). Liraglutide decreases hepatic inflammation and injury in advanced lean non-alcoholic steatohepatitis. Basic Clin. Pharmacol. Toxicol. *123*, 704–713.

Kleiner, D.E., Brunt, E.M., Van Natta, M., Behling, C., Contos, M.J., Cummings, O.W., Ferrell, L.D., Liu, Y.C., Torbenson, M.S., Unalp-Arida, A., et al. (2005). Nonalcoholic Steatohepatitis Clinical Research, Design and validation of a histological scoring system for nonalcoholic fatty liver disease. Hepatology *41*, 1313–1321.

Kojima, M., Takahashi, H., Kuwashiro, T., Tanaka, K., Mori, H., Ozaki, I., Kitajima, Y., Matsuda, Y.,

Ashida, K., Eguchi, Y., and Anzai, K. (2020). Glucagon-like peptide-1 receptor agonist prevented the progression of hepatocellular carcinoma in a mouse model of nonalcoholic steatohepatitis. Int. J. Mol. Sci. *21*, E5722.

Koo, S.H. (2013). Nonalcoholic fatty liver disease: molecular mechanisms for the hepatic steatosis. Clin. Mol. Hepatol. *19*, 210–215.

Gasmi, L., and McLennan, A.G. (2001). The mouse Nudt7 gene encodes a peroxisomal nudix hydrolase specific for coenzyme A and its derivatives. Biochem. J. *357*, 33–38.

Lee, J., Hong, S.W., Rhee, E.J., and Lee, W.Y. (2012). GLP-1 receptor agonist and non-alcoholic fatty liver disease. Diabetes Metab. J. *36*, 262–267.

Lee, S.S., Pineau, T., Drago, J., Lee, E.J., Owens, J.W., Kroetz, D.L., Fernandez-Salguero, P.M., Westphal, H., and Gonzalez, F.J. (1995). Targeted disruption of the alpha isoform of the peroxisome proliferator-activated receptor gene in mice results in abolishment of the pleiotropic effects of peroxisome proliferators. Mol. Cell Biol. *15*, 3012–3022.

Lodhi, I.J., and Semenkovich, C.F. (2014). Peroxisomes: a nexus for lipid metabolism and cellular signaling. Cell Metab. *19*, 380–392.

Lv, X., Dong, Y., Hu, L., Lu, F., Zhou, C., and Qin, S. (2020). Glucagon-like peptide-1 receptor agonists (GLP-1 RAs) for the management of nonalcoholic fatty liver disease (NAFLD): a systematic review. Endocrinol. Diabetes Metab. *3*, e00163.

Matsusue, K., Haluzik, M., Lambert, G., Yim, S.H., Gavrilova, O., Ward, J.M., Brewer, B., Jr., Reitman, M.L., and Gonzalez, F.J. (2003). Liver-specific disruption of PPARgamma in leptin-deficient mice improves fatty liver but aggravates diabetic phenotypes. J. Clin. Invest. *111*, 737–747.

Moran-Salvador, E., Lopez-Parra, M., Garcia-Alonso, V., Titos, E., Martinez-Clemente, M., Gonzalez-Periz, A., Lopez-Vicario, C., Barak, Y., Arroyo, V., and Claria, J. (2011). Role for PPARgamma in obesity-induced hepatic steatosis as determined by hepatocyte- and macrophage-specific conditional knockouts. FASEB J. *25*, 2538–2550.

Moreno-Fernandez, M.E., Giles, D.A., Stankiewicz, T.E., Sheridan, R., Karns, R., Cappelletti, M., Lampe, K., Mukherjee, R., Sina, C., Sallese, A., et al. (2018). Peroxisomal beta-oxidation regulates whole body metabolism, inflammatory vigor, and pathogenesis of nonalcoholic fatty liver disease. JCI Insight *3*, 93626.

Musso, G., Gambino, R., and Cassader, M. (2009). Recent insights into hepatic lipid metabolism in non-alcoholic fatty liver disease (NAFLD). Prog. Lipid Res. *48*, 1–26.

Neuschwander-Tetri, B.A. (2010). Hepatic lipotoxicity and the pathogenesis of nonalcoholic steatohepatitis: the central role of nontriglyceride fatty acid metabolites. Hepatology *52*, 774–788.

Onuma, H., Inukai, K., Kitahara, A., Moriya, R., Nishida, S., Tanaka, T., Katsuta, H., Takahashi,

K., Sumitani, Y., Hosaka, T., and Ishida, H. (2014). The glucagon-like peptide 1 receptor agonist enhances intrinsic peroxisome proliferator-activated receptor γ activity in endothelial cells. Biochem. Biophys. Res. Commun. *451*, 339–344.

Park, H., He, A., Tan, M., Johnson, J.M., Dean, J.M., Pietka, T.A., Chen, Y., Zhang, X., Hsu, F.F., Razani, B., et al. (2019). Peroxisome-derived lipids regulate adipose thermogenesis by mediating cold-induced mitochondrial fission. J. Clin. Invest. *129*, 694–711.

Raney, A.K., Johnson, J.L., Palmer, C.N., and McLachlan, A. (1997). Members of the nuclear receptor superfamily regulate transcription from the hepatitis B virus nucleocapsid promoter. J. Virol. *71*, 1058–1071.

Rector, R.S., Thyfault, J.P., Wei, Y., and Ibdah, J.A. (2008). Non-alcoholic fatty liver disease and the metabolic syndrome: an update. World J. Gastroenterol. *14*, 185–192.

Rolo, A.P., Teodoro, J.S., and Palmeira, C.M. (2012). Role of oxidative stress in the pathogenesis of nonalcoholic steatohepatitis. Free Radic. Biol. Med. *52*, 59–69.

Rose, N.R., and Klose, R.J. (2014). Understanding the relationship between DNA methylation and histone lysine methylation. Biochim. Biophys. Acta *1839*, 1362–1372.

Schrader, M., Costello, J., Godinho, L.F., and Islinger, M. (2015). Peroxisome-mitochondria interplay and disease. J. Inherit. Metab. Dis. *38*, 681–702.

Shai, N., Schuldiner, M., and Zalckvar, E. (2016). No peroxisome is an island - peroxisome contact sites. Biochim. Biophys. Acta *1863*, 1061–1069.

Sharma, S., and Black, S.M. (2009). Carnitine homeostasis, mitochondrial function, and cardiovascular disease, drug discovery today. Drug Discov. Today Dis. Mech. *6*, e31–e39.

Shimano, H., and Sato, R. (2017). SREBP-regulated lipid metabolism: convergent physiology - divergent pathophysiology. Nat. Rev. Endocrinol. *13*, 710–730.

Song, J., Baek, I.J., Chun, C.H., and Jin, E.J. (2018). Dysregulation of the NUDT7-PGAM1 axis is responsible for chondrocyte death during osteoarthritis pathogenesis. Nat. Commun. *9*, 3427.

Strable, M.S., and Ntambi, J.M. (2010). Genetic control of de novo lipogenesis: role in diet-induced obesity. Crit. Rev. Biochem. Mol. Biol. *45*, 199–214.

Svegliati-Baroni, G., Saccomanno, S., Rychlicki, C., Agostinelli, L., De Minicis, S., Candelaresi, C., Faraci, G., Pacetti, D., Vivarelli, M., Nicolini, D., et al. (2011). Glucagon-like peptide-1 receptor activation stimulates hepatic lipid oxidation and restores hepatic signalling alteration induced by a high-fat diet in nonalcoholic steatohepatitis. Liver Int. *31*, 1285–1297.

Tailleux, A., Wouters, K., and Staels, B. (2012). Roles of PPARs in NAFLD: potential therapeutic targets. Biochim. Biophys. Acta *1821*, 809–818.

Tamura, S., and Shimomura, I. (2005). Contribution of adipose tissue and de novo lipogenesis to nonalcoholic fatty liver disease. J. Clin. Invest. *115*, 1139–1142.

Wahli, W., and Michalik, L. (2012). PPARs at the crossroads of lipid signaling and inflammation. Trends Endocrinol. Metab. *23*, 351–363.

Wang, G., Bonkovsky, H.L., de Lemos, A., and Burczynski, F.J. (2015). Recent insights into the biological functions of liver fatty acid binding protein 1. J. Lipid Res. *56*, 2238–2247.

Westerbacka, J., Kolak, M., Kiviluoto, T., Arkkila, P., Sirén, J., Hamsten, A., Fisher, R.M., and Yki-Järvinen, H. (2007). Genes involved in fatty acid partitioning and binding, lipolysis, monocyte/macrophage recruitment, and inflammation are overexpressed in the human fatty liver of insulin-resistant subjects. Diabetes *56*, 2759–2765.

Wolf Greenstein, A., Majumdar, N., Yang, P., Subbaiah, P.V., Kineman, R.D., and Cordoba-Chacon, J. (2017). Hepatocyte-specific, PPARgamma-regulated mechanisms to promote steatosis in adult mice. J. Endocrinol. *232*, 107–121.

Zhang, Q., Xiao, X., Zheng, J., Li, M., Yu, M., Ping, F., Wang, T., and Wang, X. (2018). Liraglutide protects cardiac function in diabetic rats through the PPARalpha pathway. Biosci. Rep. *38*, BSR20180059.

STAR★METHODS

KEY RESOURCES TABLE

REAGENT or RESOURCE	SOURCE	IDENTIFIER
Antibodies		
ACOX1	Cusabio	Cat# PA617998HA01HU
H3K4me3	Abcam	Cat# ab8580; RRID:AB_306649
NUDT7	Youngin Frontier	N/A
PPARγ	Abcam	Cat# ab41928; RRID:AB_777392
FABP4	Abcam	Cat# ab92501; RRID:AB_10562486
FASN	Cell signaling technology	Cat# 3180S; RRID:AB_2100796
PMP70	Abcam	Cat# ab211533
SCD1	Abcam	Cat# ab19862; RRID:AB_445179
H3K4me2	Cell signaling technology	Cat#9725; RRID:AB_10205451
H3K27me2	Cell signaling technology	Cat#9755; RRID:AB_659841
H3K27me3	Abcam	Cat#ab6002; RRID:AB_305237
Histone H3	Cell signaling technology	Cat#4499; RRID:AB_10544537
Chemicals, peptides, and recombinant proteins		
CellMask™ Orange Plasma membrane Stain	Thermo Fisher Scientific	C10045
Oil red O	Sigma-Aldrich	Cat# O0625s
BODIPY493/503	Thermo Fisher Scientific	Cat# D3922
BODIPY581/591	Thermo Fisher Scientific	Cat# D3861
Filipin	Sigma-Aldrich	Cat# SAE0088
3rd generation packaging system	ABM	Cat# LV053
Lentifectin	ABM	Cat# G074
Lenti-X Concentrator	Clontech	Cat# PT4421-2
Critical commercial assays		
Nuclear/Cytosol Extraction Kit	BioVision	K266-100
EZ-Triglyceride Quantification Assay Kit	DoGen	Cat# DG-TGC100
EZ-Free Fatty Acid Assay Kit	DoGen	Cat # DG-FFA100
EZ-Total Cholesterol Assay Kit	DoGen	Cat# DG-TSC100
Quick Cell Proliferation Colorimetric Assay Kit	BioVision	Cat# K302-2500
Catalase Activity Colorimetric/Fluorometric Assay Kit	BioVision	Cat# K773-100
ChIP-IT Express Kit	Active Motif	Cat# 53009
Experimental models: Cell lines		
HEK-293T	ATCC	CRL-3216
Hepatocyte	This paper	N/A
Experimental models: Organisms/strains		
Mouse: Nudt7$^{+/-}$: C57BL/6N	Song et al. (2018, NComm)	N/A
Mouse: Catalse$-/-$: C57BL/6N	Generously donated by Goo Taeg Oh, Ewha Womans University	N/A
Oligonucleotides		
See Table S2 for primer sequences.		
Software and algorithms		
RStudio	RStudio	https://github.com/rstudio/rstudio

Continued		
REAGENT or RESOURCE	SOURCE	IDENTIFIER
QIAGEN's Ingenuity Pathway Analysis algorithm (IPA)	QIAGEN	www.qiagen.com/ingenuity
Gene Set Enrichment Analysis (GSEA)	Subramanian, Tamayo, et al. (2005, PNAS) and and Mootha, Lindgren, et al. (2003, Nature Genetics)	www.gsea-msigdb.org/gsea

RESOURCE AVAILABILITY

Lead contact

Further information and requests for resources and reagents should be directed to and will be fulfilled by the Lead Contact, Eun-Jung Jin (jineunjung@wku.ac.kr).

Materials availability

Materials in this study will be made available from the lead contact with a material transfer agreement.

Data and code availability

- Data reported in this paper will be shared by the lead contact upon request.
- This paper does not report original codes.
- Any additional information available from the lead contact upon request.

EXPERIMENTAL MODEL AND SUBJECT DETAILS

Ethical approval

Liver tissues were obtained from 22 patients who underwent bariatric and metabolic surgery at Keimyung University, Dongsan Hospital, between January 2019 and December 2019. The study was conducted in accordance with the Declaration of Helsinki, and the protocol was reviewed and approved by the Institutional Review Board of Keimyung University Dongsan Hospital (IRB No. 2015-01-015). Animal studies were performed following approval from the Wonkwang University Animal Care and Use Committee and were in compliance with institutional guidelines (#WKU18-23). Sample size for animal studies was determined by statistical analysis of variance and on the basis our experience with similar studies. The sample size (n) for each experimental group is indicated in the figure legends and is between three and six mice per group. All of the *in vivo* experiments were replicated at least three times by two experimentalists independently. All histological and IHC samples were blinded before the images were taken and quantified by trained liver pathologists.

Animals

NUDT7-knockout (KO) mice on a C57BL/6 background were generated by TALEN-mediated gene targeting [31]. {Song, 2018 #19}Twelve-month-old male C57BL/6N (Nudt7$^{+/+}$) and NUDT7 KO (Nudt7$^{+/-}$) mice or Catalase KO (Cat$^{-/-}$) were fed normal chow diet (NCD) ad-libitum or high-fat diet (HFD; 60% kcal from fat; Research Diets Inc.) for the indicated times. Nudt7$^{+/-}$ mice were fed a HFD for 8 weeks to induce NAFLD. Next, liraglutide (200 μg/kg) or an equal volume of sterile saline was intraperitoneal (i.p.) injected for 4 weeks. All animals were fasted for 12 h (overnight) before scarification, and blood was collected to isolate the serum for biochemical analysis.

METHOD DETAILS

Indirect calorimetry

Water and food intake, VO$_2$, VCO$_2$, and Heat were analyzed using an Oxymax system (Columbus Instruments). Mice were placed in the chambers at 23°C with free access to food and water and acclimated for more than 50 min before measurement.

Lentiviral constructs packaging and tail vein injection

Mock-control, Nudt7 and shAcox1-containing lentiviruses were produced using the 3rd generation packaging system (ABM, Richmond, BC, Canada). Lentivirus plasmids were transfected into HEK-293T cells using Lentifectin (ABM) in DMEM serum free medium (ThermoFisher Scientific) and cultured overnight. The

lentiviral particle containing supernatant was concentrated using a Lenti-X Concentrator (Clontech) and stored at −80°C. For in-vivo delivery, concentrated lentivirus supernatant was injected into the tail vein twice a week for 6 weeks.

Histological analysis

Paraffin-embedded tissues were sliced into 5 μm sections and stained with hematoxylin and eosin (H&E). Plasma membrane was stained with CellMask Orange (Thermo Fisher Scientific). Frozen liver sections were cut into 5 μm slices and stained with 0.3% Oil red O (Sigma-Aldrich) in 60% isopropanol or 0.25 mg/mL filipin. For immunohistochemistry (IHC), sections were incubated overnight at 4°C (1:200 dilution) in a humidified chamber with the following primary antibodies; ACOX1 (Cusabio), H3K4me3 (Abcam), NUDT7 (Youngin Frontier), PPARγ (Abcam), FABP4(Abcam), FASN (Cell signaling technology), PMP70 (Abcam), and SCD1 (Abcam). Positive staining was visualized using the Liquid DAB Substrate Chromogen System (Dako) combined with counterstaining with hematoxylin. Histological images were acquired with a light microscope (Leica).

Cell culture

Hepatocytes were isolated using collagenase perfusion technique from 10-week-old $Nudt7^{+/+}$ and $Nudt7^{+/-}$ mice and cultured in DMEM high glucose medium (ThermoFisher Scientific) supplemented with 10% FBS (ThermoFisher Scientific) and 100 U/ml penicillin-streptomycin (ThermoFisher Scientific).

Immunoblotting

Mouse tissues or cells were homogenized with RIPA buffer (Cell Signaling Technology) supplemented with phenylmethylsulfonyl fluoride (PMSF) protease inhibitor (Sigma-Aldrich), and nuclear lysates were extracted using a Nuclear/Cytosol Extraction Kit (BioVision). Proteins (40 μg) were separated on a sodium dodecyl sulfate (SDS)-polyacrylamide gel, transferred to a nitrocellulose membrane (GE Healthcare), and then incubated with the following primary antibodies; H3K4me2 (Cell Signaling Technology), H3K4me3 (Abcam), H3K27me2 (Cell Signaling Technology), H3K27me3 (Abcam), and histone H3 (Cell Signaling Technology). The blotted nitrocellulose membranes were developed using horseradish peroxidase-conjugated secondary antibodies (α-Rabbit or α-Mouse, 1:2500 dilution) and target proteins were detected and visualized using either an enhanced chemiluminescence (ECL) system (ThermoFisher Scientific).

Lipid and cholesterol accumulation assay

Cells were stained with 2 μM BODIPY$^{493/503}$ (ThermoFisher Scientific) or 5 μM Lipid ROS (BODIPY$^{581/591}$; ThermoFisher Scientific) or 50 μg/mL filipin (Sigma-Aldrich) to evaluate lipid accumulation, and images were captured with an Imaging System (ThermoFisher Scientific).

Mouse liver and serum analysis

Hepatic or serum TG and FFA were measured using a EZ-Triglyceride Quantification Assay Kit (DoGen) or EZ-Free Fatty Acid Assay Kit (DoGen) or EZ-Total Cholesterol Assay Kit (DoGen) according to the manufacturer's instructions. Serum aspartate transaminase (AST) and alanine transferase (ALT) were obtained from the Seoul Clinical Laboratories.

Cell proliferation and catalase activity assay

Cell proliferation and catalase activity were analyzed using Quick Cell Proliferation Colorimetric Assay Kit (BioVision) and Catalase Activity Colorimetric/Fluorometric Assay Kit (BioVision) according to the manufacturer's instructions.

qRT-PCR and peroxisomal gene profiling

Total RNA was isolated using RNAiso Plus (TaKaRa) according to the manufacturer's instructions. Then, 1 μg RNA was reverse transcribed using the 5X All-In-One RT MasterMix (Abm). Each target gene amplified with the StepOne Plus Real-Time PCR System (Applied Biosystems) using specific primers listed in Table S2 and relative expression level of each gene was normalized with Rn18s. The 42 peroxisomal genes were determined by qRT-PCR. Heatmap images and visualized using the R studio.

RNA sequencing

RNA sequencing was performed using the Illumina HiSeq 4000 System. Libraries were quantified using qRT-PCR and their quality was analyzed using the Agilent 2100 Bioanalyzer (Agilent Technologies). Raw counts were generated by calculating the fragments per kilobase of transcript per million mapped reads (FPKM) of each sample using the Cufflinks software. Data were transformed logarithmically and normalized using the quantile normalization technique.

Chromatin immunoprecipitation (ChIP) assay

The H3K4me3-ChIP assay was performed using a ChIP-IT Express Kit (Active Motif). The genomic DNA was sheared using components of the ChIP-IT Express Kit (Active Motif) and 20 μg of genomic DNA was immunoprecipitated with 3 μg of H3K4me3 antibody (Abcam) and Protein G-coupled magnetic beads (Active Motif). The bead-bound chromatin was eluted with 1% SDS and 0.1 M $NaHCO_3$ and purified using phenol-chloroform. Promoter sequences for qRT-PCR were obtained from the Eukaryotic Promoter Database (http://epd.vital-it.ch) and specific primers listed in Table S2.

Pathway analysis using GSEA and IPA

Microarray data of GSE33814 (steatosis and steatohepatitis patient liver), GSE49541 (mild NASH and advanced NASH patient liver), and GSE39549 (HFD fed mouse liver) from Gene Expression Omnibus (GEO) and RNA sequencing data of 12 month-old chow fed Nudt7$^{+/-}$ or Nudt7$^{+/+}$ mouse liver were analyzed in this study. Differentially expressed genes (DEGs) was analyzed using QIAGEN's Ingenuity Pathway Analysis algorithm (IPA, QIAGEN, www.qiagen.com/ingenuity) or Gene Set Enrichment Analysis (GSEA, http: www. broadinstitute.org/gsea).

Histology analysis and IHC of human samples

Formalin-fixed paraffin-embedded (FFPE) block specimens from intraoperative liver biopsy during bariatric surgery were obtained. All the H&E stained slides were reviewed by an experienced pathologist (HWL) who was blinded to the clinicopathological features or clinical outcome. The severity of NAFLD was evaluated histologic features according to a NAFLD activity score (NAS): steatosis, lobular inflammation, hepatocyte ballooning, and fibrosis (Kleiner et al., 2005).

Protein expressions were assessed by an immunohistochemical study. IHC staining was performed using an automated immunostainer, Ventana BenchMark XT (Ventana Medical Systems, Tucson, AZ, USA) with an UltraView kit, according to the manufacturer's protocol. NUDT7 (Ab Frontier), PPARγ (Abcam) and H3K4me3 (Abcam) were applied as the primary antibodies, after which the samples were incubated at 37°C for 32 min followed by standard Ventana signal amplification, and hematoxylin and a bluing reagent counterstaining, consecutively. After the autostainer process, the slides were mounted and examined by light microscopy. Positive staining of NUDT7 was indicated by a prominent brownish pigmentation in the cytoplasm, and PPARγ and H3K4me3 were in the nucleus. Negative controls were obtained by omitting the specific primary antibodies of the same species. Positive and negative controls stained appropriately. Expressions were assessed according to staining intensity and scored from 0 to 3 as follows: 0 (no), 1 (weak), 2 (moderate), and 3 (strong). Staining score 0 to 1 considered low expression and score 2 to 3 considered high, respectively.

QUANTIFICATION AND STATISTICAL ANALYSIS

Results are expressed as the mean $\pm$ standard error of mean (SEM). Significant differences between two groups were analyzed by Student's t-test. Differences among three or more groups were compared by one-way or two-way ANOVA followed by Tukey's multiple comparisons test. $p \leq 0.05$ was considered statistically significant.